

Development and Evaluation of a UTE-based Method for Attenuation Correction in MR-PET Neurologic Studies

Meher Juttukonda¹, Yasheng Chen², Yi Su³, Tammie Benzinger³, Brian Rubin³, David Lalush¹, and Hongyu An²

¹Biomedical Engineering, University of North Carolina, Chapel Hill, North Carolina, United States, ²Radiology, University of North Carolina, Chapel Hill, North Carolina, United States, ³Radiology, Washington University, St. Louis, Missouri, United States

Introduction: The loss of signal due to attenuation of photons in positron emission tomography (PET) can greatly diminish the quantitative accuracy of simultaneous MR-PET studies. MR-based attenuation correction has proven challenging due to the inability of traditional MR images (ex: T1- and T2-weighted) to provide the bone/air contrast necessary to derive accurate attenuation maps. This is due to the fact that attenuation is governed by a metric (linear attenuation coefficient – LAC) that depends on the electron density of tissue, whereas MR signal depends on proton density and tissue relaxation. However, recent developments in MR such as the ultra-short echo time (UTE) sequence can be used to help overcome this barrier. In this study, we have developed and evaluated a novel MR bone/air segmentation method for use in MR-based PET attenuation correction (AC).

Methods: T1-weighted MR (T1-w), CT, and dual ultra-short echo-time (UTE) images ($TE_1 = 0.07$ ms, $TE_2 = 2.46$ ms) from 20 patients were used in this study. For each patient's data set, the UTE and CT images were rigidly registered to the T1-w image and the following protocol was followed. For soft-tissue, a threshold of UTE_1 was employed followed by morphological operations to fill the gaps. To classify bone voxels, the UTE_1 and UTE_2 images were used to calculate an estimate of the transverse relaxation rate parameter $R2^*$. Since bone has a higher relaxation rate than other tissues, a simple threshold (i.e. 0.06) was applied to the $R2^*$ image to define bone voxels. To classify air voxels, the reciprocal of the UTE_1 image ($1/UTE_1$) was computed. Since air voxels exhibit near-zero signal in the UTE_1 image while all other tissues have considerably larger signal, the reciprocal operation greatly enhances air voxels compared to surrounding regions. A fixed threshold of 0.06 was used to segment air across all patients. A brain mask obtained from the T1-w image was then used to remove any misclassified tissue within the brain. To evaluate the accuracy of the segmentation, dice coefficients were computed for the bone and air tissue classes with respect to a CT-based segmentation method described in literature¹ for a range of slices where registration between MR and CT was deemed sufficiently accurate. In addition, realistic, patient-specific PET simulations were conducted to evaluate the accuracy of the attenuation maps derived from the proposed segmentation method. Attenuation maps were generated by assigning LACs of 0.151 cm^{-1} , 0.096 cm^{-1} , and 0 cm^{-1} to voxels classified as bone, soft tissue and air, respectively¹. In the simulations, attenuation was applied using a map derived from bilinear scaling of the

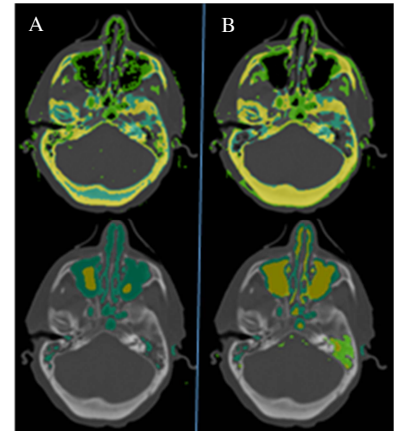


Figure 1: The MR-based segmentations (green) for bone (top row) and air (bottom row) are shown with CTseg (blue) and “regions of overlap for the DUseg method (panel A) and R2seg method (panel B).

CT image², widely considered the gold standard. The attenuated data was then corrected using maps derived from each of 3 methods: the proposed $R2^*$ -based method (R2seg), the CT-based segmentation method (CTseg), and another UTE-based segmentation method (DUseg) previously described in literature¹. To evaluate the accuracy of the AC methods, percent-error maps of the simulated PET images were generated and compared to images that were reconstructed using the gold standard scaled-CT for AC. The mean absolute percent-error (MAPE) was calculated in regions of brain tissue for each patient and compared across all 3 methods.

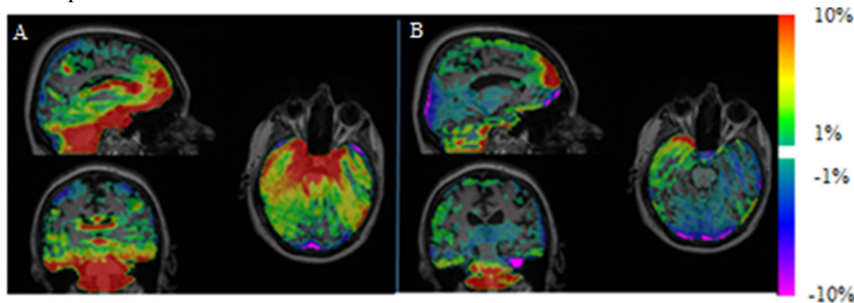


Figure 2: Percent-error maps in sagittal, axial, and coronal views (clockwise from top left) of simulated PET images compared to scaled-CT, overlaid on T1-w images for one patient. Panel A shows the error maps for the DUseg method, while Panel B shows the error maps for the R2seg method. Errors with $\pm 1\%$ have been set to 0% to allow for better visualization of larger errors.

CTseg method is considered the silver standard and has the best performance in AC among segmentation-based methods¹. While the proposed method is not statistically as accurate as the CTseg method ($p < 0.01$), it performs significantly better than the DUseg method ($p < 0.01$). In addition, the relatively sparse distribution of large-error regions for the R2seg method compared to the DUseg method can be seen in Fig 2. The large overestimation of PET signal seen in the DUseg method in regions of brain near the sinus cavities can be attributed to the misclassification of air voxels.

Discussion: The results of this study show that the proposed $R2^*$ -based segmentation method outperforms a published method in the segmentation of bone and air as demonstrated by the improved dice coefficients. As expected, the better bone/air/tissue segmentation leads to significant improvement in PET AC accuracy as well. In addition, the performance of our method is more consistent across patients compared to the DUseg method. Since the $R2^*$ computation uses a ratio of the UTE images, signal variation across different patients and acquisitions can be minimized in the bone segmentation. Air space shows near-zero signal and is also independent of the signal variations present within surrounding tissue. Therefore, a fixed threshold on $1/UTE_1$ can readily identify air space across patients and acquisitions. Recently, a probabilistic atlas-assisted approach was introduced to improve the DUseg method and good reproducibility was demonstrated^{3,4}. This approach could be incorporated into our proposed method as well. Finally, information from this segmentation could help atlas-based methods in deriving more accurate attenuation maps and will be explored in future work.

References:

- 1) Catana et al, *J Nucl Med*. 2010; 51(9): 1431-1438.
- 2) Bai et al, *IEEE Transactions on Nuclear Science*. 2003; 50(5): 1500-1515.
- 3) Poynton et al, *Soc Nucl Med* 2012.
- 4) Chen et al, *ISMRM* 2013.